Modeling extinction and reignition in turbulent nonpremixed combustion using a doubly-conditional moment closure approach

Chong M. Cha[a)]
Center for Turbulence Research, Stanford University, Stanford, California 94305-3030

George Kosály
University of Washington, Seattle, Washington 98195-2600

Heinz Pitsch
Center for Turbulence Research, Stanford University, Stanford, California 94305-3030

(Received 9 February 2001; accepted 7 September 2001)

The scalar dissipation rate is introduced as a second conditioning variable into the first-moment, singly conditional moment closure model to describe extinction and reignition effects in turbulent, nonpremixed combustion. *A priori* testing of the combustion model using direct numerical simulation experiments exhibiting local extinction/reignition events is described. The singly conditional moment closure model is either unable to describe the extinction seen in the numerical experiments or predicts global extinction when it does not occur. The new doubly conditional moment closure approach is able to describe the extinction seen on average, but predicts the onset of reignition too early. © *2001 American Institute of Physics.* [DOI: 10.1063/1.1415426]

I. INTRODUCTION

The accurate treatment of extinction and reignition phenomena is thought to be an important factor in determining how flame stabilization occurs in practical, nonpremixed combustion systems.[1] In the joint probability density function (PDF) approach,[2,3] extinction/reignition can be treated with improved mixing models.[4] However, joint PDF methods employ a Monte Carlo type solution procedure and thus become computationally expensive when many species increase the dimensionality of the modeled joint PDF evolution equation. Presumed PDF approaches, such as flamelet modeling [1,5,6] and conditional moment closure modeling,[7–9] can be computationally tractable when many species are to be described, as is generally the case in problems of practical importance. First-order flamelet modeling and conditional moment closure modeling with singly conditional, first-moment closure breaks down when extinction and/or reignition phenomena are present.[1,9] Our focus in the present paper concerns extensions of first-order conditional moment closure modeling to describe extinction/reignition.

Currently, a fundamental closure approximation in singly conditional moment closure modeling is first-order closure of the average nonlinear chemical source terms, $\dot{\mathbf{w}}$, conditioned on the mixture fraction, $\xi(t,\mathbf{x})=\eta$:

$$\langle \dot{\mathbf{w}}(\mathbf{Y}(t,\mathbf{x}),T(t,\mathbf{x}),\rho(t,\mathbf{x}))\,|\,\xi(t,\mathbf{x})=\eta\rangle \approx \dot{\mathbf{w}}(\langle \mathbf{Y}|\,\eta\rangle,\langle T|\,\eta\rangle,\langle \rho|\,\eta\rangle),$$

where $\mathbf{Y}$ is the vector of mass fractions of the reacting species, T and ρ are the temperature and density of the mixture, respectively, and η is the sample space variable of ξ. The first-order closure approximation is not valid when fluctuations about the conditional means become significant. Figure 1 shows local extinction/reignition events in ξ space from (i) experiments of a turbulent methane/air reacting jet[10] and (ii) direct numerical simulation (DNS) of a single-step chemical reaction in spatially homogeneous and isotropic turbulence.[11] In Fig. 1, θ is the reduced temperature,

$$\theta \equiv \frac{T-T_\infty}{T_f-T_\infty},$$

with T_f the adiabatic flame temperature and T_∞ the reference temperature. The data of Fig. 1(i) is a current benchmark dataset for competing combustion models. Figure 1(i) shows the data from an entire planar cross section in the ''near-field'' of the jet, 15 diameters from the fuel nozzle. Figure 1(ii) shows the data after one-half a large-eddy turnover time ($t^* \equiv t/\tau_{\text{eddy}} = \frac{1}{2}$) from the initial, nonpremixed state. The time is nondimensionalized with the initial large-eddy turnover time, τ_{eddy}. In both subplots (i) and (ii), T_∞ was assigned the temperature of the two initially segregated fluids: the fuel and oxidizer. The temperatures of the fuel and oxidizer are the same in each of the two experiments. The highest temperatures and largest fluctuations appear where fuel and oxidizer are in stoichiometric proportion at $\xi=\xi_{\text{st}}$. (For the jet flame, $\xi_{\text{st}}=0.351$ and for the DNS, $\xi_{\text{st}}=0.5$.) Figure 1 illustrates how extinction/reignition events appear as large fluctuations about $\langle \theta|\eta\rangle$. In the present paper we focus on the DNS experimental data, as some important quantities of interest for testing the combustion model to be presented is not currently available from the jet flame experiments.

To account for the fluctuations of $\mathbf{Y}$ and θ not accounted for by the fluctuations of ξ, second-order closure of the conditional chemical source term has been proposed to improve singly conditional moment closure modeling and is currently

a)Telephone: 650-725-6635; fax: 650-723-9617. Electronic mail: chongcha@stanford.edu

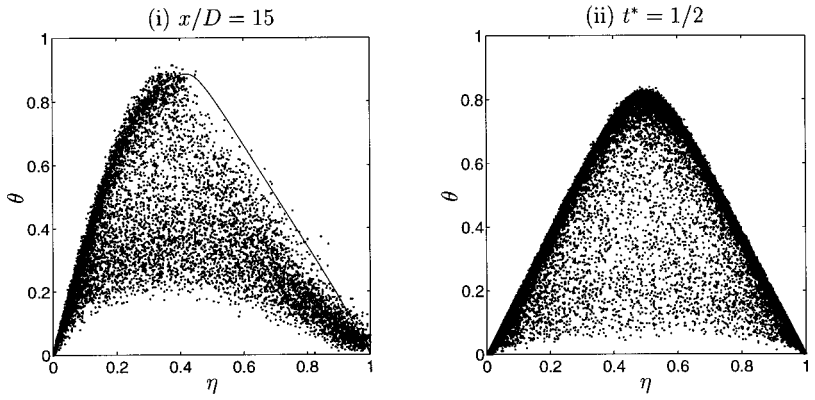

FIG. 1. Motivation of the work: Scatter plots of the reduced temperature from (i) a planar cut at $x/D=15$ of the piloted methane/air turbulent reacting jet F of Barlow and Frank (Ref. 10), and (ii) from a direct numerical simulation (DNS) of turbulence in a box of Sripakagorn (Ref. 11) at $t^* \equiv t/\tau_{\text{eddy}} = \frac{1}{2}$ with a single-step, reversible reaction. Here D is the jet nozzle diameter, τ_{eddy} is the initial large-eddy turnover time. In (i), the stoichiometric value of the mixture fraction is $\xi_{\text{st}} = 0.351$; in (ii), $\xi_{\text{st}} = 0.5$.

in development.[12,13] In the present paper we introduce the use of the dissipation rate of the scalar ξ as a second conditioning variable while maintaining the first-moment closure of the chemical source term. The scalar dissipation rate is defined as

$$\chi \equiv 2\mathcal{D}(\nabla \xi)^2,$$

where $\mathcal{D}$ is the molecular diffusivity of the mixture fraction. Figure 2 (subplot $t^* = \frac{1}{2}$) shows the DNS data of Fig. 1(ii) mapped into the scalar dissipation rate phase space at ξ

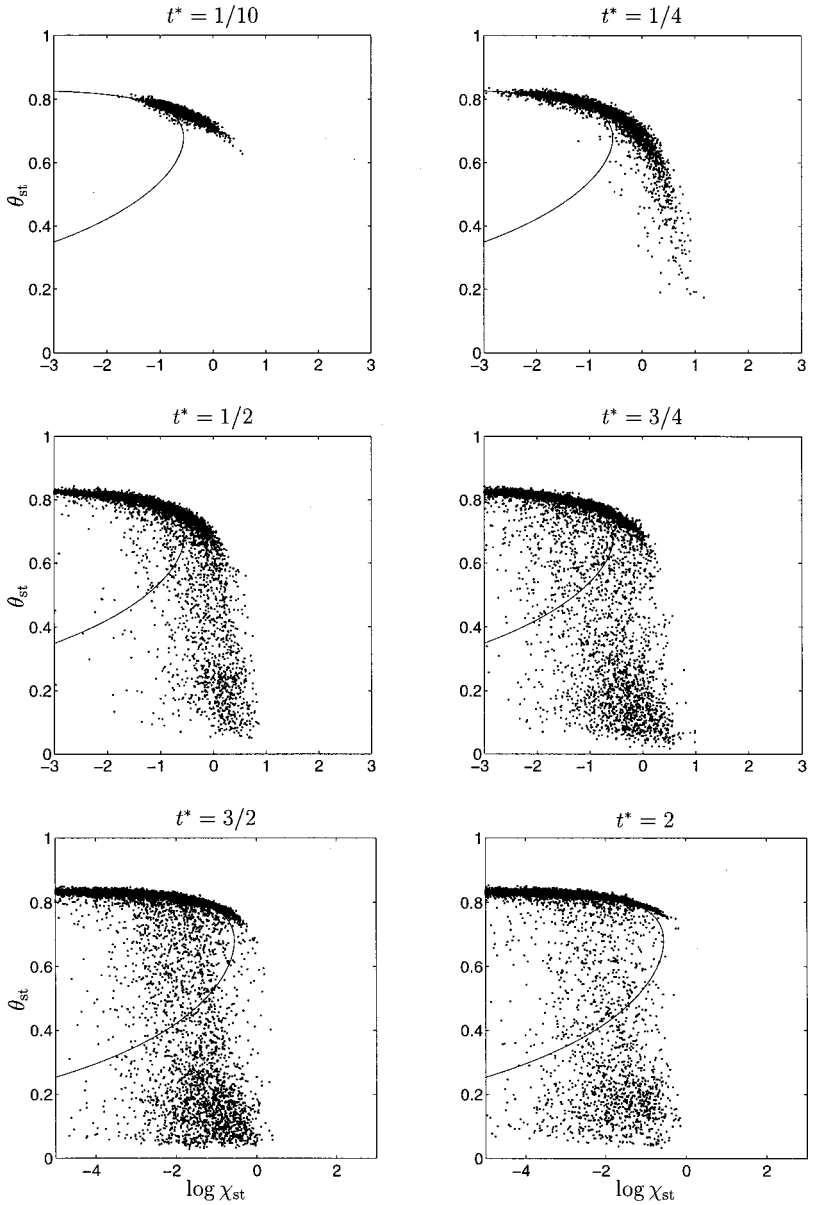

FIG. 2. The DNS experiment of spatially isotropic, homogeneous, and decaying turbulence performed by Sripakagorn (Ref. 11) for case B (cf. Table I). The reduced temperature is shown at $\xi_{\text{st}} = 0.5$ as a function of the local scalar dissipation rate, $\chi \equiv 2\mathcal{D}(\nabla \xi)^2$.

$=\xi_{st}$. (Figure 2 is described in detail later.) Measurements of χ do not yet exist for the laboratory experimental data shown in subplot (i). Note that information showing the maximum departures from equilibrium after the mapping to χ phase space is not lost. Important additional information, not discernable in ξ phase space alone, is discussed later. The presumption is that the extinction/reignition events, seen in Fig. 1 for example, can be described in the space of χ (in addition to ξ and $\mathbf{x}$).

The present formulation of introducing a second conditioning variable should be distinguished from the multiply conditional moment closure modeling in Ref. 9, where additional conditioning variables must be introduced to treat a multistream mixing problem. Here, only a two-stream mixing process is considered, where the advantage of doubly conditioning expectations (in addition to the mixture fraction) is to account for additional fluctuations about the singly conditional means due to the fluctuations of χ.

The paper is organized as follows. In the next section, the DNS experiments to be modeled are described. In Sec. III, the assumptions of singly conditional moment closure modeling are reviewed and a new conditional moment closure model, where the scalar dissipation rate is introduced as a second conditioning variable is formulated. In Sec. IV, *a priori* modeling comparisons are made with the DNS experiments. Finally, in the conclusions section, the strengths and limitation of the doubly conditional moment closure model are summarized.

II. NUMERICAL EXPERIMENT

Presently, the *a priori* combustion modeling comparisons are made with the DNS experiments performed by Sripakagorn.[11] Briefly, fuel (F), oxidizer (O), and product (P) involved in a one-step, second-order, reversible reaction,

$$\mathrm{F}+\mathrm{O}\underset{k/K}{\overset{k}{\rightleftharpoons}}2\mathrm{P}, \tag{2.1}$$

evolve in isotropic, homogeneous, and decaying turbulence. The stoichiometric value of the mixture fraction is $\xi_{st}=0.5$. The forward reaction rate, k, in Eq. (2.1) has an Arrhenius temperature dependence with the equilibrium constant, K, held fixed. The production rates for fuel, oxidizer, and product are $\dot{w}_F=-\dot{w}$, $\dot{w}_O=-\dot{w}$, and $\dot{w}_P=2\dot{w}$, respectively, where

$$\dot{w}(Y_F,Y_O,Y_P,\theta)=A\exp\left(-\frac{\mathrm{Ze}}{\alpha}\right)\exp\left(-\frac{\mathrm{Ze}(1-\theta)}{1-\alpha(1-\theta)}\right)\times\left(Y_FY_O-\frac{1}{K}Y_P^2\right)$$

is the reaction rate. Here, A is the frequency factor (multiplied by density and divided by molecular weight, assumed equal for all species), $\alpha\equiv(T_f-T_\infty)/T_f$ is the heat release parameter, $\mathrm{Ze}\equiv\alpha T_a/T_f$ is the Zeldovich number, and T_a is the activation temperature. The Schmidt number is 0.7 and Lewis numbers unity. The turbulent flow is incompressible and the molecular diffusivities and viscosity are independent of the temperature (cf. Sripakagorn[11] for details of the simulation). Use of such an idealized system to decouple and investigate presumed PDF combustion modeling strategies is common.[14,15]

TABLE I. Variation of the DNS cases of Sripakagorn (Ref. 11), where the reaction $\mathrm{F}+\mathrm{O}\underset{k/K}{\overset{k}{\rightleftharpoons}}2\mathrm{P}$ is simulated in decaying, homogeneous, and isotropic turbulence with an initial $\mathrm{Re}_\lambda=33$ on a 128^3 grid. Here $\mathrm{Sc}=0.7$ and Lewis numbers are unity. Chemistry rate parameters are $\alpha=0.87$, $\mathrm{Ze}=4$, and $K=100$.

Case	A (s^{-1})	χ_q (s^{-1})
A	13.0×10^4	0.94
B	8.0×10^4	0.57
C	0.3×10^4	0.21

Figure 2 shows the level of extinction/reignition from the DNS experiment with $A=8\times10^4\,\mathrm{s}^{-1}$, $\alpha=0.87$, $\mathrm{Ze}=4$, and $K=100$. The solid line in each subplot is the steady-state solution of the flamelet equation[5] for θ at ξ_{st}. The quenching value of the scalar dissipation rate at ξ_{st} is $\chi_q=0.57\,\mathrm{s}^{-1}$ for this moderate extinction level case. Additional cases were performed where the degree of extinction was increased and decreased from the moderate extinction level case shown Fig. 2 by varying the frequency factor A. The experimental cases considered in this paper are summarized in Table I. Figure 2 corresponds to case B.

Some preliminary qualitative observations are made that are important for later discussion. In all three cases, the average scalar dissipation rate at ξ_{st}, $\langle\chi_{st}\rangle$, increases to a maximum at $t^*\approx\frac{1}{4}$, then decays in time. The fluctuating scalar dissipation rate is approximately lognormal in distribution and maximum local values of χ_{st} also correspond to this time, as can be seen in Fig. 2. Figure 2 shows that for $t^*\lesssim\frac{1}{2}$, extinction events occur when the local values of χ_{st} exceed χ_q. Local extinction events reduce the conditionally averaged mean temperature. For increasing times $t^*>\frac{1}{2}$, both extinction and reignition events occur simultaneously. Reignition can only occur when local values of χ_{st} are less than χ_q. Reignition dominates at late times, as very few local values of χ_{st} ever exceed the quenching value. An important consequence of the overlapping of extinction and reignition events is noted. The number of local reignition events must dominate the level of extinction before the conditionally averaged temperature at ξ_{st} can increase. Consequently, prior to this increase, many local reignition events occur while the conditionally averaged temperature is still decreasing.

III. COMBUSTION MODELING

A. Singly conditional moment closure

In this section, we review the singly conditional moment closure model, which is to be used as a baseline comparison against the strategy of doubly conditioning.

For the present case of a single-step reaction, the conditional averages of all species and temperature can be obtained from the single equation for the average of θ singly conditioned on ξ:

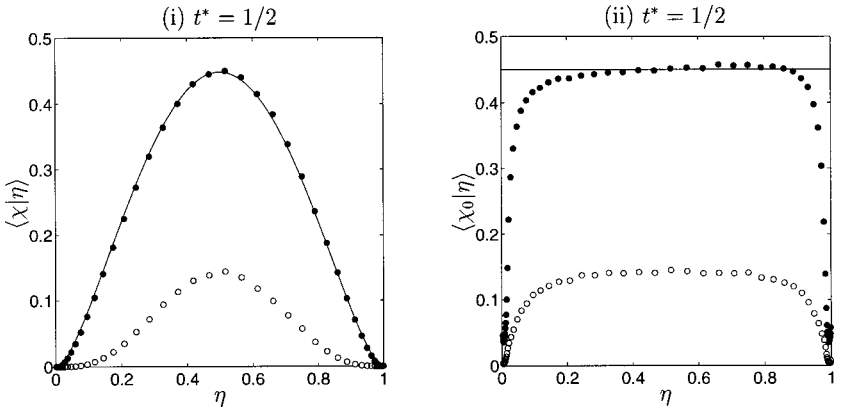

FIG. 3. An illustration of (i) the $\langle\chi|\eta\rangle\equiv\langle\chi_0\rangle F(\eta)$ dependence in the present DNS experiment with $F(\eta)\equiv\exp\{-2[\mathrm{erf}^{-1}(2\eta-1)]^2\}$, and (ii) the approximate independence of $\chi_0\equiv\chi/F$ with ξ. The variance is represented by the open circles. Note, $\chi_0=\chi$ at $\xi_{st}=0.5$ for the present case.

$$\frac{\partial}{\partial t}\Theta=\frac{\langle\chi|\eta\rangle}{2}\frac{\partial^2}{\partial\eta^2}\Theta+2\dot{w}(Q_F,Q_O,Q_P,\Theta), \tag{3.1}$$

where $\langle\chi|\eta\rangle$ is the conditionally averaged scalar dissipation rate, $Q_F=\eta-Q_P/2$, $Q_O=1-\eta-Q_P/2$, and $Q_P=\Theta$. Equation (3.1) is referred to as the cmc1 model throughout the remainder of the paper. With appropriate initial and boundary conditions, closure is obtained with $\langle\chi|\eta\rangle$ specified directly from the DNS (to be described in Sec. III C). Details of the derivation are found in Klimenko and Bilger.[9] Briefly, we have the following.

(1) Terms representing the diffusion of the conditional averages in physical space,

$$\frac{e_Q}{\rho}\equiv\left\langle\left(\mathcal{D}\nabla^2\Theta+2\mathcal{D}\boldsymbol{\nabla}\xi\cdot\boldsymbol{\nabla}\frac{\partial\Theta}{\partial\eta}\right)\middle|\,\eta\right\rangle,$$

have been ignored in Eq. (3.1) (e_Q closure).

(2) A closure hypothesis involving contributions to the balance of the conditional average by fluctuations about singly conditional means, $\theta'\equiv\theta-\Theta$, has been invoked:

$$\frac{e_Y}{\rho}\equiv\left\langle\left(\frac{\partial}{\partial t}+\mathbf{u}\cdot\boldsymbol{\nabla}-\mathcal{D}\nabla^2\right)\theta'\middle|\,\eta\right\rangle=-\frac{\boldsymbol{\nabla}\cdot(\langle\mathbf{u}'\theta'|\eta\rangle p_\xi)}{p_\xi}$$

(e_Y closure). Here $\mathbf{u}(t,\mathbf{x})$ is the turbulent velocity field in physical space, $\mathbf{u}'$ its fluctuations about the mean, and $p_\xi(\eta;t)$ the PDF of ξ.

(3) The reaction rate is represented by singly conditional means only (first-moment $\dot{w}$ closure).

Assumption (1) is strictly valid only at high Reynolds numbers in nonhomogeneous (shear) flows,[9] has been shown to be valid at low Reynolds numbers for a semihomogeneous flow,[16] and is exact for the present spatially degenerate (homogeneous, isotropic) case. The closure hypothesis invoked in (2) has been validated against a DNS database of a temporal mixing layer.[17] For the present fully homogeneous DNS case, the e_Y term can be ignored under this closure hypothesis. Assumption (3) is valid when fluctuations about singly conditional means are small and thus higher-order terms negligible in an expansion of the nonlinear chemical source term.[9] In doubly conditional moment closure, a second conditioning variable is chosen that tries to account for these fluctuations not attributable to ξ.

B. Doubly conditional moment closure

The physical significance of the scalar dissipation rate, χ, in extinction/reignition phenomena is well known from flamelet modeling.[6] In first-order flamelet modeling, $\theta(t,\xi;\chi)$, where χ appears as a random parameter. Along the isocontour of ξ_{st} then, fluctuations of $\theta(t,\xi_{st})$ are due to the random fluctuations of χ. Here χ is approximately lognormal in distribution and so its fluctuations become larger with increasing χ. Hence, at larger values of χ, fluctuations of θ are also correspondingly larger relative to the fluctuations of θ at smaller values of χ. The effect of large χ on θ is illustrated in the DNS experiment shown in Fig. 2, where for most of the times, large fluctuations of θ correspond to relatively large values of χ. Accounting for fluctuations of θ due to χ is done by choosing χ as the second conditioning variable in a conditional moment closure modeling framework.

Presently, we choose $\chi_0\equiv\chi/F(\xi)$ as the second conditioning variable. This specializes the combustion modeling to the present DNS experiments where ξ and χ_0 have been found to be statistically independent with

$$F(\xi)\equiv\exp\{-2[\mathrm{erf}^{-1}(2\xi-1)]^2\}. \tag{3.2}$$

Note, $\chi_0=\chi$ at $\xi_{st}=0.5$ for the present case. Figure 3 shows the typical functional dependence of the conditional mean (filled circles) and standard deviation (open circles) of χ and χ_0 with the mixture fraction. Subplot (ii) illustrates the approximate independence of the first two moments of χ_0 with η, implying the approximate statistical independence of the random variables χ_0 and ξ.

The ξ functional dependence of F in Eq. (3.2) to render χ_0 independent of ξ can be shown using mapping closure.[18] For the present spatially degenerate case with a symmetric double-delta-function initial condition for the PDF of ξ,[19] an analytic expression for the mixture fraction dependence of the nth conditional moment of χ can be shown to be $\langle\chi^n|\xi=\eta\rangle\sim F^n(\eta)$ with $F(\eta)=\exp\{-2[\mathrm{erf}^{-1}(2\eta-1)]^2\}$. Direct substitution of $\chi=\chi_0F(\xi)$ into $\langle\chi^n|\xi=\eta\rangle$ yields the desired result that $\langle\chi_0^n|\xi=\eta\rangle$, the nth conditional moment of χ_0, is independent of η, and thus χ_0 and ξ are statistically independent. The mapping closure model becomes invalid at the final stages of mixing.[20] For the times of interest investigated in the present paper, the variance is sufficiently large such

that the PDF of ξ is approximately or nearly always bimodal and the ξ functional given by Eq. (3.2) holds, as predicted by mapping closure.

The formulation of the doubly conditional moment closure model does not require the statistical independence of ξ and the second conditioning variable, but simplifies its implementation (to be described in Sec. III C) and the modeling of the joint PDF of ξ and the second conditioning variable required to obtain unconditioned averages (e.g., the averaged density to be used in a Reynolds-averaged or large-eddy simulation). In high Reynolds number flows, the decomposition $\chi=\chi_0 F(\xi)$ would not be necessary as χ is independent of ξ,[21] and χ could replace χ_0 in the derivation of the doubly conditional moment closure model to follow.

The source term for the scalar dissipation rate is required to derive the governing equations for the conditional averages of the reacting scalars. Here χ is produced by the turbulent velocity field, which can increase the scalar gradients by the effect of strain, and is destroyed by the action of molecular diffusion, which relax the gradients of ξ. These effects are represented by the terms on the rhs of the transport equation for χ,[22] which, for the present case of constant ρ and $\mathcal{D}$, can be written as

$$\frac{L(\chi)}{\rho}\equiv\left(\frac{\partial}{\partial t}+\mathbf{u}\cdot\boldsymbol{\nabla}-\mathcal{D}\nabla^2\right)\chi=S_\chi, \tag{3.3a}$$

with

$$S_\chi\equiv -4\mathcal{D}(\boldsymbol{\nabla}\xi\otimes\boldsymbol{\nabla}\xi):(\boldsymbol{\nabla}\otimes\mathbf{u}) -4\mathcal{D}^2(\boldsymbol{\nabla}\otimes\boldsymbol{\nabla}\xi):(\boldsymbol{\nabla}\otimes\boldsymbol{\nabla}\xi). \tag{3.3b}$$

Here, $\otimes$ is the dyadic product of two vectors. The source term for χ_0 can be obtained by substituting $\chi=\chi_0 F(\xi)$ into Eq. (3.3a). Making use of the relation $\boldsymbol{\nabla}(\chi_0 F)=\chi_0\boldsymbol{\nabla}F+\boldsymbol{\nabla}\chi_0 F$ with $\boldsymbol{\nabla}F=\boldsymbol{\nabla}\xi dF/d\xi$, the transport equation for χ_0 can be shown to be

$$\frac{L(\chi_0)}{\rho}=\frac{S_\chi}{F}+\frac{2\mathcal{D}\boldsymbol{\nabla}\xi\cdot\boldsymbol{\nabla}\chi_0}{F}\frac{dF}{d\xi}+\frac{\chi_0^2}{2}\frac{d^2F}{d\xi^2}, \tag{3.3c}$$

where S_χ is the source term for χ given by Eq. (3.3b) and, for convenience, the lhs operator $L(\ )$ defined in Eq. (3.3a) is used. For example, $L(\xi)=0$ as ξ is a conserved scalar.

Following the decomposition procedure,[9] the doubly conditional moment closure equations with ξ and χ_0 as conditioning variables can be derived using the differentiation rules:

$$\frac{\partial\theta}{\partial t}=\frac{\partial\Theta}{\partial t}+\frac{\partial\Theta}{\partial\eta}\frac{\partial\xi}{\partial t}+\frac{\partial\Theta}{\partial X}\frac{\partial\chi_0}{\partial t}+\frac{\partial\theta'}{\partial t},$$

$$\boldsymbol{\nabla}\theta=\boldsymbol{\nabla}\Theta+\frac{\partial\Theta}{\partial\eta}\boldsymbol{\nabla}\xi+\frac{\partial\Theta}{\partial X}\boldsymbol{\nabla}\chi_0+\boldsymbol{\nabla}\theta'.$$

Here, θ' represents fluctuations about the doubly conditional mean $\langle\theta|\eta,X\rangle=\Theta$ with X the corresponding sample space variable for χ_0. Substitution into the local, instantaneous governing equation for the normalized temperature, $L(\theta)=2\dot{w}$, yields

$$\begin{aligned}\frac{L(\Theta)}{\rho}+\frac{L(\xi)}{\rho}\frac{\partial\Theta}{\partial\eta}+\frac{L(\chi_0)}{\rho}\frac{\partial\Theta}{\partial X}&=2\mathcal{D}\boldsymbol{\nabla}\xi\cdot\boldsymbol{\nabla}\frac{\partial\Theta}{\partial\eta}+2\mathcal{D}\boldsymbol{\nabla}\chi_0\cdot\boldsymbol{\nabla}\frac{\partial\Theta}{\partial X}-\frac{L(\theta')}{\rho}\\&+\mathcal{D}(\boldsymbol{\nabla}\xi)^2\frac{\partial^2\Theta}{\partial\eta^2}+2\mathcal{D}\boldsymbol{\nabla}\xi\cdot\boldsymbol{\nabla}\xi_0\frac{\partial^2\Theta}{\partial\eta\partial X}\\&+\mathcal{D}(\boldsymbol{\nabla}\chi_0)^2\frac{\partial^2\Theta}{\partial X^2}+2\dot{w}.\end{aligned}$$

Noting that $L(\xi)=0$ in the second term on the lhs and $\mathcal{D}(\boldsymbol{\nabla}\xi)^2=\chi/2$ in the fourth term on the rhs, taking the doubly conditional average of this equation gives

$$\begin{aligned}\frac{\partial\Theta}{dt}+\langle S_\chi|\eta,X\rangle\frac{\partial\Theta}{\partial X}=\frac{e_Q}{\rho}+\frac{e_Y}{\rho}+\langle 2\dot{w}|\eta,X\rangle&+\left\langle\frac{X}{2}\middle|\eta,X\right\rangle\frac{\partial^2\Theta}{\partial\eta^2}\\&+\langle 2\mathcal{D}\boldsymbol{\nabla}\xi\cdot\boldsymbol{\nabla}\chi_0|\eta,X\rangle\frac{\partial^2\Theta}{\partial\eta\partial X}\\&+\langle\mathcal{D}(\boldsymbol{\nabla}\chi_0)^2|\eta,X\rangle\frac{\partial^2\Theta}{\partial X^2},\end{aligned}$$

$$\frac{e_Q}{\rho}\equiv\left\langle\left(\mathcal{D}\nabla^2\Theta+2\mathcal{D}\boldsymbol{\nabla}\xi\cdot\boldsymbol{\nabla}\frac{\partial\Theta}{\partial\eta}+2\mathcal{D}\boldsymbol{\nabla}\chi_0\cdot\boldsymbol{\nabla}\frac{\partial\Theta}{\partial X}\right)\middle|\eta,X\right\rangle,$$

$$\frac{e_Y}{\rho}\equiv\left\langle\left(\frac{\partial}{\partial t}+\mathbf{u}\cdot\boldsymbol{\nabla}-\mathcal{D}\nabla^2\right)\theta'\middle|\eta,X\right\rangle.$$

Written this way, similar unclosed terms involving fluctuations about the conditional means result as in the derivation of the singly conditional moment closure model equations;[9] namely, e_Q, e_Y, and closure of the conditionally averaged $\dot{w}$. Following the derivation given in Ref. 9, the analogous closure hypothesis for e_Y can readily be generalized for the present, doubly conditional case, leading to

$$\frac{e_Y}{\rho}=-\frac{\boldsymbol{\nabla}\cdot(\langle\mathbf{u}'\theta'|\eta,X\rangle p_\xi p_{\chi_0})}{p_\xi p_{\chi_0}},$$

with $\mathbf{u}'=\mathbf{u}-\langle\mathbf{u}|\eta,X\rangle$ and ξ and χ_0 statistically independent. Then, simplifying for the present case, the analogous terms e_Q and e_Y under double conditioning can again be neglected based on spatial homogeneity (cf. Sec. III B). With regard to first-moment $\dot{w}$ closure, the fluctuations about doubly conditioned means are presumably reduced and their neglect a more accurate approximation. That is, first-moment closure of the chemical reaction rate using doubly conditioned

means is expected to yield improved results over the analogous closure with singly conditioned means used in Eq. (3.1). These closures yield

$$\left(\frac{\partial}{\partial t}+\alpha_0\frac{\partial}{\partial X}\right)\Theta=\left(\frac{XF}{2}\frac{\partial^2}{\partial\eta^2}+\beta_0\frac{\partial^2}{\partial X^2}+\gamma_0\frac{\partial^2}{\partial\eta\partial X}\right)\Theta + 2\dot{w}(Q_F,Q_O,Q_P,\Theta), \tag{3.4a}$$

$$\alpha_0\equiv\frac{\langle S_\chi|\eta,X\rangle}{F}+\frac{1}{F}\frac{dF}{d\eta}\gamma_0+\frac{1}{2}X^2\frac{d^2F}{d\eta^2}, \tag{3.4b}$$

$$\beta_0\equiv\langle\mathcal{D}(\nabla\chi_0)^2|\eta,X\rangle, \tag{3.4c}$$

$$\gamma_0\equiv\langle 2\mathcal{D}\nabla\xi\cdot\nabla\chi_0|\eta,X\rangle, \tag{3.4d}$$

for the doubly conditional moment closure modeling governing equations. Again, for the present simplified chemistry case, $Q_F=\eta-Q_P/2$, $Q_O=1-\eta-Q_P/2$, and $Q_P=\Theta$.

The doubly conditional mean Θ in Eq. (3.4), henceforth termed model cmc2, is to be distinguished from the singly conditional means of model cmc1. Noteworthy differences between the two models are highlighted. The convection term in χ_0 phase space [the second term on the left-hand side of Eq. (3.4a)] results from the fact that χ_0 is not a conserved scalar. The nonconstant coefficient α_0 is the doubly conditional average of the source term for χ_0, which was given in Eq. (3.3c). In contrast to singly conditional moment closure, the coefficient of the diffusion term in ξ phase space [the first term on the right-hand side of Eq. (3.4a)] is closed. The second and third terms on the right-hand side of Eq. (3.4a) are additional diffusion terms that account for additional conduction losses important at high values of χ_0. These terms do not appear in singly conditional moment closure modeling, as transport in χ_0 phase space is ignored. The coefficients for these additional terms, β_0 and γ_0, are taken from the DNS (described next in Sec. III C).

C. Implementation issues

The statistical independence of ξ and χ_0 bring about simplifications in the implementation of both cmc1 and cmc2 models. Details of the implementation of the *a priori* testing of the models is described in this section.

All coefficients in Eqs. (3.1) and (3.4) are calculated directly from the DNS experiment. The conditional averages of the data are computed using an equal number of data points per bin as opposed to using equally spaced increments of the sample space variable for each bin size. In the former method, the bin size over the range in the sample space variable can differ from bin to bin, while in the latter case, each bin size would be equal by definition and could correspond to the computational mesh chosen for ξ and/or χ_0 space. The latter method can degrade the confidence of some of the conditionally averaged points, as it does not guarantee a sufficient number of data points to compute averages (or any higher-order statistics for that matter). The implemented binning procedure results in more accurate and smoother conditional averages but requires interpolation for a fixed finite-differenced computational mesh that does not change in time. Cubic interpolation is used in ξ and χ_0 space on a fixed computational grid, where the conditionally averaged DNS data are not available. The conditionally averaged coefficients of the DNS data do not change very rapidly with time and need not be computed at each time step used in the numerical integration of Eqs. (3.1) and (3.4). Cubic splines are used to interpolate the one-dimensional $\langle\chi|\eta\rangle$ profile for the cmc1 model and the two-dimensional profiles α_0, β_0, and γ_0 for the cmc2 model between 12 stations over the total time span of interest, $2\tau_{\text{eddy}}$.

Boundary conditions for the singly conditional case (at $\eta=0,1$) are $\Theta(t,0)=\Theta(t,1)=0$. For the doubly conditional case, boundary conditions must be specified for $\eta\in[0,1]$ at $X=X_{\min},X_{\max}$ and for $X\in[X_{\min},X_{\max}]$ at $\eta=0,1$. Here $\Theta(t,0,X)=\Theta(t,1,X)=0$; at $X_{\min}\approx 0$, equilibrium solutions are used while pure mixing solutions are used at some $X_{\max}\gg\chi_q$. Here χ_q is the quenching value of the scalar dissipation rate. A value of $X_{\max}=\exp(3)$ was found to be large enough to not influence solutions. Cubic interpolation is also used to fit the DNS data at the initial time in (η,X) space for the initial conditions.

Figure 3(i) shows a typical profile illustrating the η dependence of $\langle\chi|\eta\rangle$. $\langle\chi|\eta\rangle$ is taken directly from the DNS data for the singly conditional moment modeling calculations. Singly conditional moment modeling calculations show no appreciable effect on the solutions with $\langle\chi|\eta\rangle$ modeled as $\langle\chi_0\rangle F(\eta)$ (cf. Fig. 3). This modeling has been used in all cmc1 results to follow.

Figures 4 and 5 show the ξ and χ_0 dependence of the coefficients α_0, β_0, and γ_0 (round symbols). Also shown are the analogous coefficients if χ were used as the second conditioning variable (square symbols): $\langle S_\chi|\xi=\eta,\chi=X\rangle$ (analogous to α_0, but with second conditioning on χ instead of χ_0), $\langle\mathcal{D}(\nabla\chi)^2|\xi=\eta,\chi=X\rangle$ (analogous to β_0), and $\langle 2\mathcal{D}\nabla\xi\cdot\nabla\chi|\xi=\eta,\chi=X\rangle$ (analogous to γ_0). At $\xi=\xi_{\text{st}}$, Fig. 4 shows the X dependence of α_0 and $\langle S_\chi|\xi=\xi_{\text{st}},\chi=X\rangle$ (top row) and β_0 and $\langle\mathcal{D}(\nabla\chi)^2|\xi=\xi_{\text{st}},\chi=X\rangle$ (bottom row). Here γ_0 and $\langle 2\mathcal{D}\nabla\xi\cdot\nabla\chi|\xi=\xi_{\text{st}},\chi=X\rangle$ are independent of X and are not shown. At χ or $\chi_0=\langle\chi_{\text{st}}\rangle\equiv X_1$, Fig. 5 shows the η dependence of α_0 and $\langle S_\chi|\xi=\eta,\chi=X_1\rangle$ (top row), β_0 and $\langle\mathcal{D}(\nabla\chi)^2|\xi=\eta,\chi=X_1\rangle$ (middle row), and γ_0 and $\langle 2\mathcal{D}\nabla\xi\cdot\nabla\chi|\xi=\eta,\chi=X_1\rangle$ (bottom row). The figure shows that α_0, β_0, and γ_0 are approximately independent of η, further corroborating the independence of χ_0 and ξ. For example, the functional dependence of $\langle(|\nabla\chi_0|)|\eta,X\rangle$ depend less on η than $\langle(|\nabla\chi|)|\eta,X\rangle$. Doubly conditional moment modeling calculations with and without the cross derivative term, $\partial^2\Theta/\partial\eta\partial X$ (corresponding to the assumption of $\gamma_0=0$), shows no appreciable effect on the solutions. Hence, only values for α_0 and β_0 need to be specified on the X boundaries of the computational mesh. At $X_{\min}$, both are set to zero; at $X_{\max}$, $\alpha_0=0$ and a value for β_0 is extrapolated from a power law fit of the data.

D. Practical implementation

The doubly conditional moment closure model as an *a posteriori* predictive modeling tool is briefly summarized as

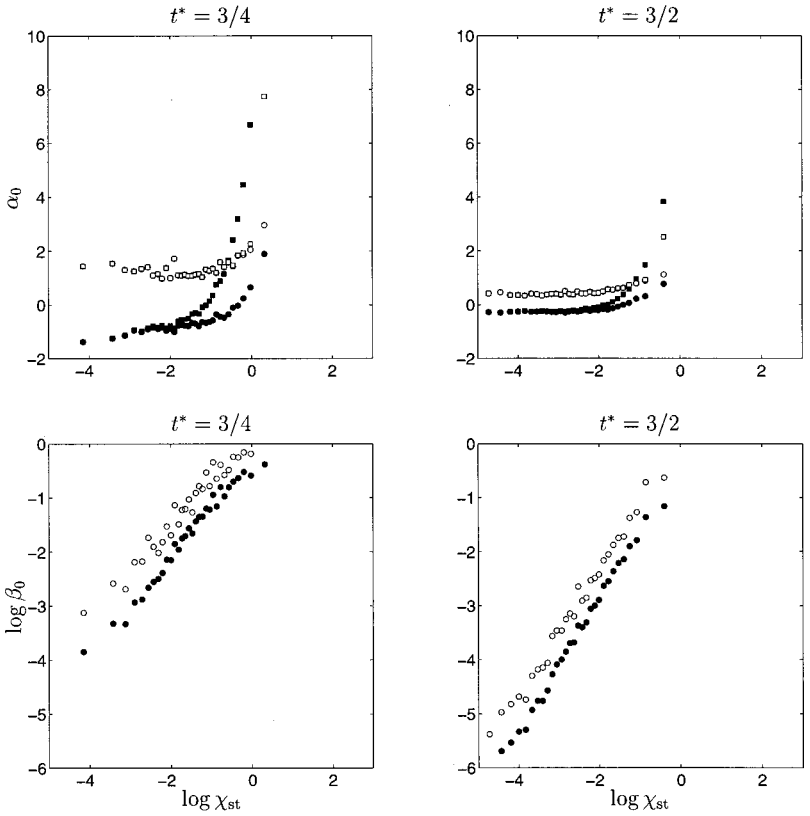

FIG. 4. Scalar dissipation rate dependence of the coefficients in doubly conditional moment closure modeling (at $\xi=\xi_{st}$): α_0 and β_0 (circles) and $\langle S_\chi|\xi=\xi_{st},\chi=X\rangle$ (note conditioning on χ, not χ_0) and $\langle \mathcal{D}(\nabla\chi)^2|\xi=\xi_{st},\chi=X\rangle$ (squares). Open symbols are corresponding rms information.

compared and contrasted to singly conditional moment closure modeling for high Reynolds number turbulent reacting flows, e.g., the jet flame of Fig. 1(i).

Analogous to cmc1, an extension of cmc2 to incorporate complex chemistry is a trivial task and involves simultaneous solutions of $NS+1$ equations taking the form of Eq. (3.4). $NS+1$ is the total number of reacting species plus the additional equation for temperature. Concurrently (unconditioned) Favre-averaged equations would be solved for the turbulent velocity and mixture fraction fields with a suitable turbulence model. Various submodels are employed to relate unconditional to conditional averages (to specify the coefficients in the conditional moment closure equations) and construct presumed PDF shapes of the conditioning variable(s) (to convolve the conditionally averaged density and temperature for the fluid dynamic calculations).

Numerous approaches exist to describe the conditionally averaged coefficients. The simplest of methods include replacing the conditional averages with their unconditionally averaged density-weighted counterparts.[23] In more elaborate methods, Fredholm integral equations are inverted, assuming a form for the joint PDF of the conditioning variable(s).[24,25] The former class of methods would require no modification to specify all coefficients in the doubly conditional moment governing equations, while the latter method has already been applied to two conditional averages in the framework of conditional source term estimation.[25] The only additional information required by cmc2 then is the (unconditioned) Favre-averages of α_0, β_0, and γ_0 in Eq. (3.4) with χ_0 replaced by χ and a submodel to specify the PDF of χ. Note for high Reynolds numbers, χ can be assumed to be statistically independent of ξ (cf. a previous discussion in Sec. III B).

The modeling of Favre-averaged nonreacting scalars and their gradients has been developed by Jones and others[26] in relation to a transport equation for $\langle\rho\chi\rangle/\langle\rho\rangle\equiv\tilde{\chi}$ (and hence also $\tilde{\alpha}_0$, the Favre-averaged source term in transport equation for $\tilde{\chi}$). An extension of their work to explicitly model $\tilde{\beta}_0$ and $\tilde{\gamma}_0$ would be necessary. A two-parameter presumed beta PDF shape for ξ are commonly applied to practical flows, where only the mean and variance of the mixture fraction, $\tilde{\xi}$ and $\widetilde{\xi''^2}$, determine all the statistics of ξ. Laboratory experiments[27] suggest that the lognormal distribution of χ may be characterized by only its mean, $\tilde{\chi}$. Thus, the joint PDF of ξ and χ, $p_{\xi\chi}$, can be specified everywhere by

$$p_{\xi\chi}(\eta,X;t,\mathbf{x})=p_\xi[\eta;\tilde{\xi}(t,\mathbf{x}),\widetilde{\xi''^2}(t,\mathbf{x})]p_\chi[X;\tilde{\chi}(t,\mathbf{x})],$$

where p_ξ and p_χ are the marginal beta PDF for ξ and lognormal PDF for χ, respectively.

In summary, the required modeling efforts to practically apply cmc2 include the development/validation of models for $\tilde{\beta}_0$ and $\tilde{\gamma}_0$ and validation of the model for $p_{\xi\chi}$. These modeling efforts fall under the rubric of turbulence modeling (of a nonreacting scalar). Presumed PDF combustion modeling approaches, like cmc1, and cmc2, can be validated independent of turbulence modeling issues by working in phase space. The present DNS experiments are more suited for *a priori* combustion modeling due to the Reynolds number restriction.

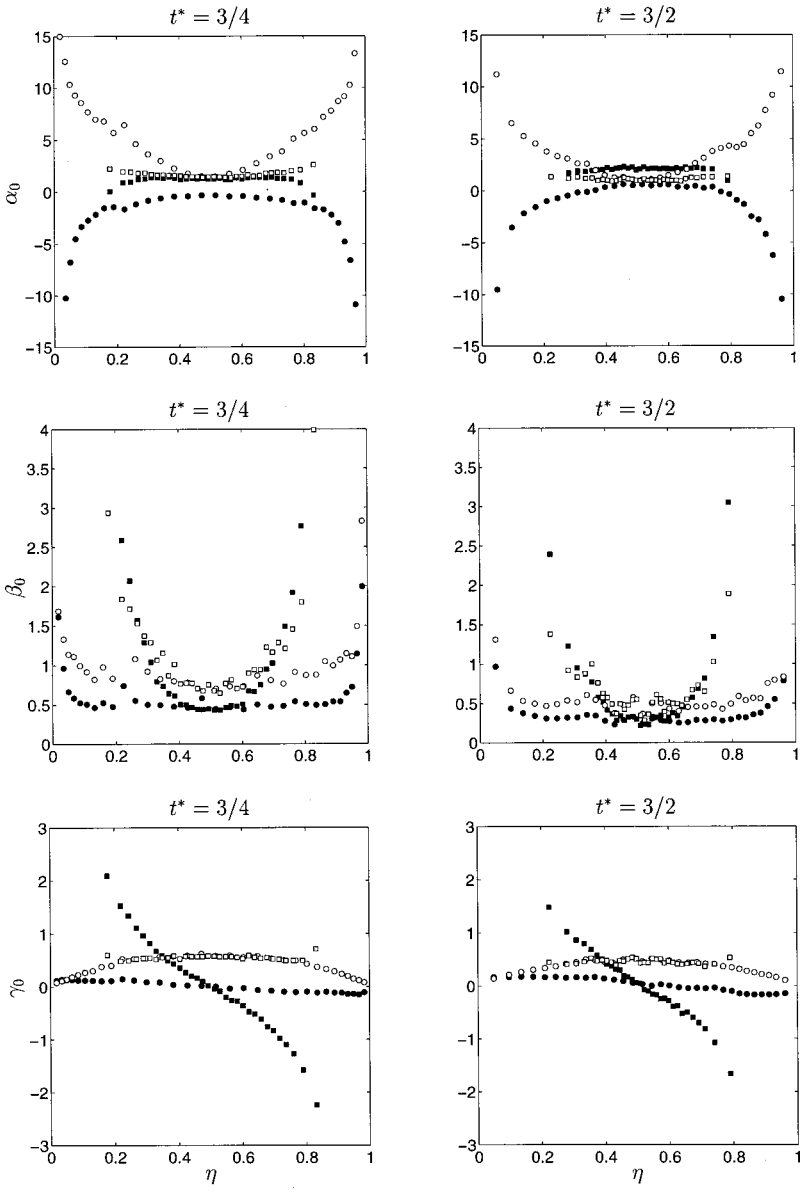

FIG. 5. Mixture fraction dependence of the coefficients in doubly conditional moment closure modeling (at $X = X_1 \equiv \langle \chi_0 \rangle$): α_0, β_0, and γ_0 (circles) and $\langle S_\chi | \xi = \eta, \chi = X_1 \rangle$ (note conditioning on χ, not χ_0), $\langle \mathcal{D}(\nabla \chi)^2 | \xi = \eta, \chi = X_1 \rangle$, and $\langle 2\mathcal{D} \nabla \xi \cdot \nabla \chi | \xi = \eta, \chi = X_1 \rangle$ (squares). Open symbols are corresponding rms information.

IV. RESULTS AND DISCUSSION

The qualitative observations made with regard to Fig. 2 at the end of Sec. II describe the important role the scalar dissipation rate plays in the extinction and reignition events occurring in the DNS experiments: (i) Extinction occurs when the local value of χ exceeds the quenching value, χ_q; (ii) reignition only occurs when χ has locally fallen below this value; and (iii) both local extinction and reignition events can occur at the same time.

With regard to (i) and (ii), cmc2 modeling describes extinction by accounting for χ_0 fluctuations and describes reignition by transport in χ_0 phase space. In cmc1, only averaged scalar dissipation rate information appears and the effect of locally large values of χ at ξ_{st} are neglected. The expectation is that the extinction events seen in Fig. 2 (case B), for example, cannot be adequately described by the cmc1 model. Case C was designed such that most of the local values of χ_{st} exceed χ_q. (Here $\langle \chi | \xi_{\mathrm{st}} \rangle$ exceeds χ_q over one initial large-eddy turnover time in case C.) As is well known, a serious deficiency of the cmc1 model is its inability to reignite when $\langle \chi | \xi_{\mathrm{st}} \rangle$ exceeds χ_q for a sufficient period of time.

With regard to (ii) and (iii), the observations made regarding reignition events in the DNS experiments do not specify the physical mechanism by which reignition takes place but only states that it is conditional on the event that locally χ must be less than χ_q. That is, there is no guarantee that reignition should be adequately described by transport in χ_0 phase space alone, the only mechanism by which it can occur in cmc2 modeling. No mechanism for reignition exists in cmc1. It is important to note that the reignition mechanism(s) not accounted for by cmc2 modeling could lead to deviations between the predictions and the DNS data, even when the conditionally averaged temperature is decreasing due to the existence of overlapping reignition events. This should not be misconstrued as shortcomings in the ability of cmc2 to describe extinction, which can confidently be attributed to locally large fluctuations of the scalar dissipation rate

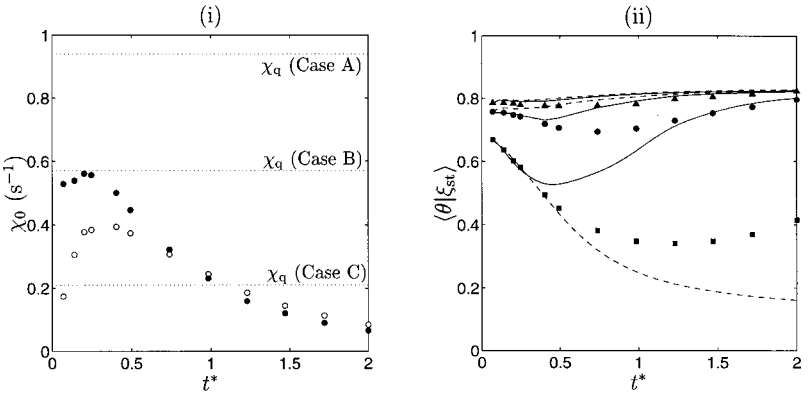

FIG. 6. (i) The average scalar dissipation rate at ξ_{st}, $\langle\chi_0\rangle$ (filled circles), and its rms, $\chi_0' \equiv \sqrt{\langle\chi_0'^2\rangle}$ (open circles), from the DNS experimental cases. A dot–dot line corresponds to χ_q for each case (cf. Table I). (ii) Singly conditional mean of the product at ξ_{st}: triangles=case A; circles=case B; squares=case C; dash–dash line=cmc1 modeling predictions and solid line=cmc2 calculations.

following the observations of the experimental DNS data that were made with regard to Fig. 2 in Sec. II. This must be kept in mind when gauging the true merits of cmc2 modeling over the cmc1 model in the results and discussion to follow.

Figure 6(i) shows the average scalar dissipation rate at ξ_{st}, $\langle\chi_0\rangle$ (filled circles), and its rms, $\sqrt{\langle\chi_0'^2\rangle} \equiv \chi_0'$ (open circles), identical for all three DNS experimental cases a–c (cf. Table I). The dot–dot line corresponds to χ_q for each case. Subplot (ii) of Fig. 6 shows cmc1 (dash–dash line) and cmc2 (solid line) modeling results against the DNS data (triangles=case A, circles=case B, squares=case C) of the average reduced temperature conditional on the events $\xi = \xi_{st}$. The doubly conditional moment closure solutions have been convolved with the probability density function (pdf) of χ_0.

$$\langle\theta|\xi_{st}\rangle = \int_0^\infty \Theta(t,\xi_{st},X) p_{\chi_0}(X;t)\,dX,$$

where $p_{\chi 0}$ is the pdf of χ_0 taken from the DNS experimental data and Θ is the solution of Eq. (3.4).

Case A corresponds to a case with low extinction levels, as the frequency factor for this case was chosen such that the quenching value of the scalar dissipation rate was relatively large, $\chi_q = \max\langle\chi_0\rangle + \max\chi_0'$ [cf. Table I and Fig. 6(i)]. Thus, most of the fluctuations of χ_0 are unimportant with respect to extinction and therefore also reignition. The singly and doubly conditional moment closure modeling predictions are comparable for this case and deviate little from the data.

In case B, $\chi_q \approx \max\langle\chi_0\rangle$ and the singly conditional modeling results do not predict the extinction that occurs in the mean for $t^* \lesssim \frac{1}{2}$. The doubly conditional moment closure model is able to describe the extinction at these relatively early times, but predicts the onset of reignition too soon (or, alternatively, the level of temperature depression is underpredicted for later times $t^* > \frac{1}{2}$).

Case C corresponds to a case with relatively high extinction levels as $\chi_q = \max\langle\chi_0\rangle - \max\chi_0'$. In this case, the cmc1 model predicts complete (global) extinction, whereas the numerical experiment exhibits a recovery to a burning state. No mechanism exists in the cmc1 model to allow for reignition. The cmc2 model can reignite *via* the transport in χ_0 phase space. However, the reignition predicted by cmc2 modeling again occurs too early, as was also observed in case B.

The strengths and weaknesses of the cmc2 model can be understood by considering the doubly conditional statistics. Case B is used as an illustrative case. Figure 7 shows cmc1 (dash-dash line) and cmc2 (solid line) modeling results against the DNS data (symbols). Comparisons are made for increasing times from $t^* = \frac{1}{4}$ (top row of subplots) to $t^* = \frac{3}{2}$ (bottom row) and conditional on three representative values of the scalar dissipation rate: a relatively low value (left column of subplots), moderate (center column), and a relatively high value (right column). More precisely, the center column of subplots are conditioned on the events $X = \langle\chi_0\rangle$, $X = \langle\chi_0\rangle - \chi_0'$ in the left column, and $X = \langle\chi_0\rangle + \chi_0'$ in the right column of subplots. [Figure 6(i) shows $\langle\chi_0\rangle$ (filled circles) and χ_0' (open circles) at the various times.] Recall that $\langle\chi_0\rangle$ is the only required mixing information to be used by the cmc1 model. In contrast, cmc2 modeling accounts for all values of χ_0, including those greater and smaller than $\langle\chi_0\rangle$. Open symbols are doubly conditioned rms information of θ taken from the DNS experiment. As can also be seen from Fig. 2, the rms of θ (open circles in Fig. 7) increases with time (moving from the top row down in Fig. 7) and higher scalar dissipation rates (moving from the left column to the right in Fig. 7).

For all times, both singly and doubly conditional moment closure models are comparable at relatively low values of X with respect to $\langle\chi_0\rangle$ (left column of subplots in Fig. 7), where the effects of extinction are not significant in the mean, and represent the data well.

For times $t^* \lesssim \frac{1}{2}$ and at relatively high scalar dissipation rate values with respect to $\langle\chi_0\rangle$ [subplots (iii) and (vi) in Fig. 7], the cmc2 model yields the most significant improvement over the singly conditional moment closure results. For this case, the mean value of χ_0 never exceeds χ_q in the DNS experiment [cf. Fig. 6(i)], hence the singly conditional modeling results could never predict any extinction events. cmc2 modeling accounts for the fluctuations of χ_0, which can exceed χ_q by over a factor of 5 (see Fig. 2 at $t^* = \frac{1}{4}$, for example), and thus can yield the improved predictions seen in subplots (iii) and (vi) of Fig. 7 at the relatively large $X \gtrsim \chi_q$. Recall from Fig. 2 that reignition events are rare at these times.

For increasing times, $t^* > \frac{1}{2}$ (bottom half of Fig. 7), when reignition occurs in the mean, the doubly conditional modeling results diverge from the data [witness subplots (ix) and

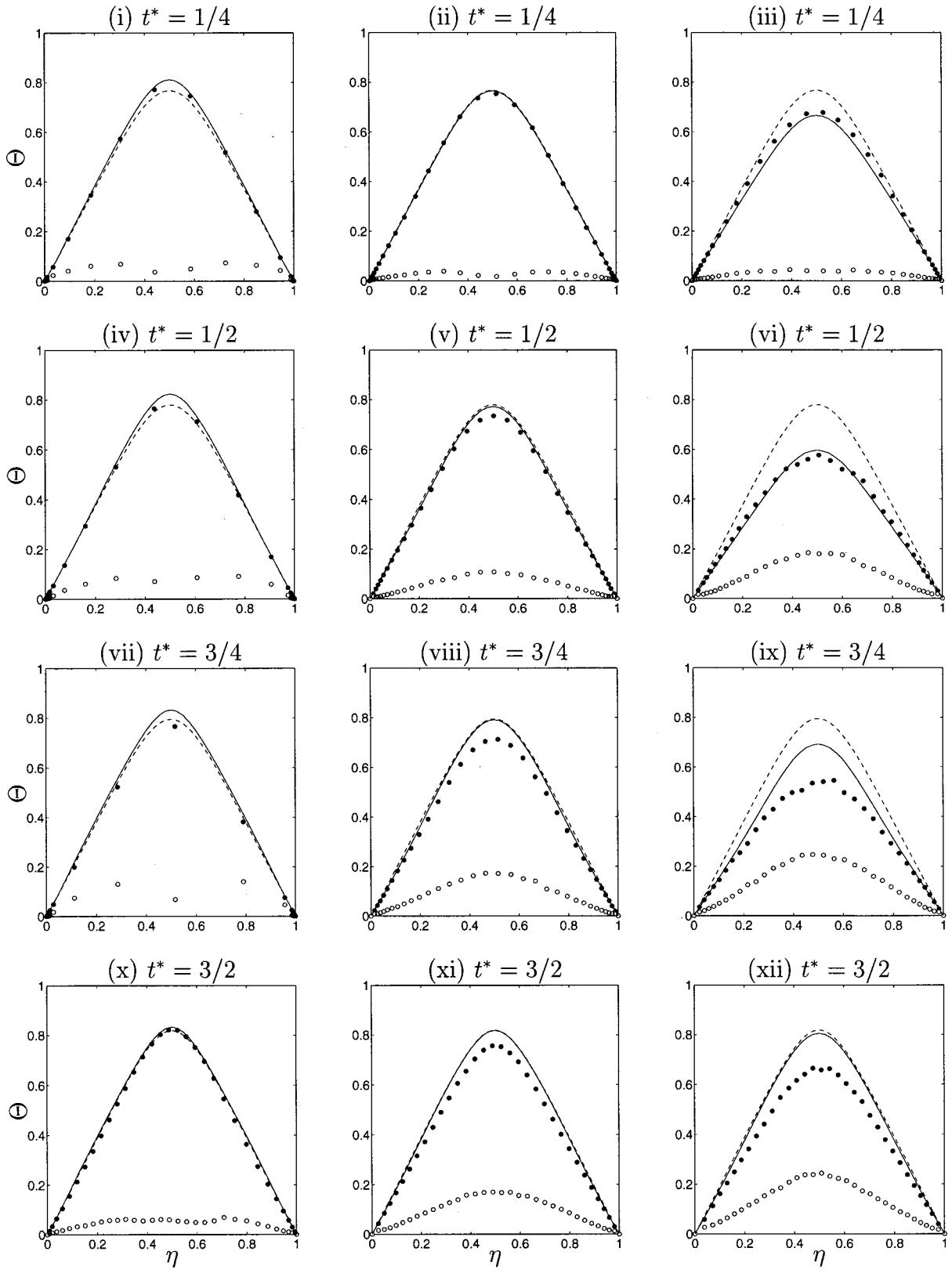

FIG. 7. Modeling comparisons: Symbols=DNS data, dash–dash line=cmc1; solid line=cmc2. Left column: conditioning on relatively low values of χ_0 ($X=\langle\chi_0\rangle-\sqrt{\langle\chi_0'^2\rangle}$), center column=conditioning at $X=\langle\chi_0\rangle$, right column: conditioning on relatively high values of χ_0 ($X=\langle\chi_0\rangle+\sqrt{\langle\chi_0'^2\rangle}$). Open symbols are corresponding rms information.

(xii) in Fig. 7]. Both $\langle\chi_0\rangle$ and χ_0' decay in time. The values of the scalar dissipation rate at times $t^*>\frac{1}{2}$ is evidently insufficient to account for the reduction in the conditional mean, which is comparable, for example, in subplot (ix) versus (vi). The diffusion in X space in the cmc2 model is evidently also insufficient to yield the required reduction in the conditional means. This may be due to the neglect of the influence of the fluctuations of the dissipation rate of the

scalar dissipation rate, β_0, the coefficient of the diffusion term in X space [cf. Eq. (3.4)]. (The present doubly conditional moment closure model also neglects fluctuations about α_0 and γ_0, which could also contribute to enhanced diffusion in the scalar dissipation rate space.) In any case, the shortcomings of the cmc2 model are due to the fluctuations about the doubly conditioned means not accounted for by the fluctuations of ξ and χ_0 (and as represented by the rms of θ seen in Fig. 7). When these fluctuations become significant [subplots (ix) and (xii) in Fig. 7, for example], the doubly conditional moment closure model underpredicts the level to which the temperature is depressed in the experiment. Recall from Fig. 2 that significant reignition events begin to occur locally at these times as more and more local values of the scalar dissipation rate fall below χ_q.

The cause of these large conditional fluctuations of θ at relatively low values of the scalar dissipation rate with respect to χ_q are due to the local reignition events that become more and more frequent for times $t^* > \frac{1}{2}$ and dominate at late times (as observed in Sec. II with regard to Fig. 2). Recall that these reignition events begin to occur before the conditionally averaged mean temperature reaches its minimum value. Evidently, the mechanism by which reignition is accounted for by the present cmc2 model [cf. the discussion regarding points (ii) and (iii) at the beginning of this section] allows these reignition events to occur too quickly. This should not belittle the advancements made by the new model, however, which correctly applies the physically viable mechanisms (derived from the experimental observations made in Sec. II) by which extinction occurs and reignition is allowed to occur.

V. CONCLUSIONS

The singly conditional moment closure model is unable to describe the extinction and reignition seen on average in the current DNS experiments. A new conditional moment closure strategy using the scalar dissipation rate as a second conditioning variable describes extinction in the mean well, but predicts the onset of reignition too early. Strengths of the doubly conditional moment closure model also includes the ability to correctly predict the transition to a reignited state while the singly conditional analog incorrectly predicts global extinction. The weakness of the new model is due to significant fluctuations about the doubly conditional means, which can occur at low values of the scalar dissipation rate with respect to the quenching value in the (numerical) experiments.

ACKNOWLEDGMENTS

The authors express gratitude to Paiboon Sripakagorn for making available to us his DNS database before publication. G.K. is indebted to CTR for partial support of his 1999–2000 sabbatical stay at Stanford and acknowledges partial support by the National Science Foundation (NSF) under Grant No. CTS-9810103. H.P. acknowledges support by the Department of Energy (DOE) under the ASCI program.

[1] N. Peters, *Turbulent Combustion* (Cambridge University Press, Cambridge, 2000).
[2] S. B. Pope, "PDF methods for turbulent reacting flows," Prog. Energy Combust. Sci. **11**, 119 (1985).
[3] C. Dopazo, "Recent developments in PDF methods," in *Turbulent Reacting Flows* (Academic, New York, 1994), Chap. 7, pp. 375–474.
[4] J. Xu and S. B. Pope, "PDF calculations of turbulent nonpremixed flames with local extinction," Combust. Flame **123**, 281 (2000).
[5] N. Peters, "Local quenching due to flame stretch in non-premixed turbulent combustion," Combust. Sci. Technol. **30**, 1 (1983).
[6] N. Peters, "Laminar diffusion flamelet models in non-premixed turbulent combustion," Prog. Energy Combust. Sci. **10**, 319 (1984).
[7] A. Yu. Klimenko, "Multicomponent diffusion of various admixtures in turbulent flow," Fluid Dyn. **25**, 327 (1990).
[8] R. W. Bilger, "Conditional moment closure for turbulent reacting flow," Phys. Fluids A **5**, 436 (1993).
[9] A. Yu. Klimenko and R. W. Bilger, "Conditional moment closure for turbulent combustion," Prog. Energy Combust. Sci. **25**, 595 (1999).
[10] R. S. Barlow and J. H. Frank, "Effects of turbulence on species mass fractions in methane/air jet flames," in *27th Symposium (International) on Combustion* (The Combustion Institute, Pittsburgh, 1998), p. 1087.
[11] P. Sripakagorn, G. Kosály, and H. Pitsch, "Local extinction–reignition in turbulent nonpremixed combustion," in *CTR Annual Research Briefs* (Center for Turbulence Research, Stanford University, 2000), pp. 117–128.
[12] N. Swaminathan and R. W. Bilger, "Conditional variance equation and its analysis," in Ref. 10, pp. 1191–1198.
[13] E. Mastorakos and R. W. Bilger, "Second-order conditional moment closure for the autoignition of turbulent flows," Phys. Fluids **10**, 1246 (1998).
[14] W. E. Mell, V. Nilsen, G. Kosály, and J. J. Riley, "Investigation of closure models for nonpremixed turbulent reacting flows," Phys. Fluids **6**, 1331 (1994).
[15] A. W. Cook, J. J. Riley, and G. Kosály, "A laminar flamelet approach to subgrid-scale chemistry in turbulent flows," Combust. Flame **109**, 332 (1997).
[16] W. K. Bushe, R. W. Bilger, and G. R. Ruetsch, "Direct numerical simulation of nonpremixed combustion with realistic chemistry," in *CTR Manuscript 173*, Center for Turbulence Research, Stanford University, March, 1999.
[17] W. K. Bushe and R. W. Bilger, "Conditional moment closure modeling of turbulent nonpremixed combustion with reduced chemistry," in Ref. 11, pp. 139–154.
[18] H. Chen, S. Chen, and R. H. Kraichnan, "Probability distribution of a stochastically advected scalar field," Phys. Rev. Lett. **63**, 2657 (1989).
[19] E. E. O'Brien and T. L. Jiang, "The conditional dissipation rate of an initially binary scalar in homogeneous turbulence," Phys. Fluids A **3**, 3121 (1991).
[20] S. S. Girimaji, "A mapping closure for turbulent scalar mixing using a time-evolving reference field," Phys. Fluids A **4**, 2875 (1992).
[21] M. R. Overholt and S. B. Pope, "Direct numerical simulation of a passive scalar with an imposed mean gradient in isotropic turbulence," Phys. Fluids **8**, 3128 (1996).
[22] G. R. Ruetsch and M. R. Maxey, "The evolution of small-scale structures in homogeneous isotropic turbulence," Phys. Fluids A **4**, 2747 (1992).
[23] C. M. Cha and G. Kosály, "Quasi-steady modeling of turbulent nonpremixed combustion," Combust. Flame **122**, 400 (2000).
[24] H. Pitsch and H. Steiner, "Scalar mixing and dissipation rate in large-eddy simulations of non-premixed turbulent combustion," in *28th Symposium (International) on Combustion* (The Combustion Institute, Pittsburgh, 2000), pp. 41–49.
[25] W. K. Bushe and H. Steiner, "Conditional moment closure for large eddy simulation of nonpremixed turbulent reacting flows," Phys. Fluids **11**, 1896 (1999).
[26] W. P. Jones, "Turbulence modeling and numerical solution methods for variable density and combusting flows," in *Turbulent Reacting Flows* (Academic, New York, 1994), pp. 309–374.
[27] E. Effelsberg and N. Peters, "Scalar dissipation rates in turbulent jets and jet diffusion flames," in *22nd Symposium (International) on Combustion* (The Combustion Institute, Pittsburgh, 1988), pp. 693–700.